Advances in Colloid and Interface Science 286 (2020) 102312

Contents lists available at ScienceDirect

Advances in Colloid and Interface Science

journal homepage: www.elsevier.com/locate/cis

Historical Perspective

The behavior of graphene oxide trapped at the air water interface

David López-Diaz [1], M. Dolores Merchán, M. Mercedes Velázquez *

Departamento de Química Física, Facultad de Ciencias Químicas, Universidad de Salamanca, 37008 Salamanca, Spain

ARTICLE INFO

Article history:
6 August 2020
28 October 2020
29 October 2020
Available online 02 November 2020

Keywords:
Graphene oxide
Purified graphene oxide
Oxidative debris
Langmuir film
Surface activity

ABSTRACT

Graphene oxide is a derivate of graphene obtained by oxidation of graphite and other carbonaceous materials. The more accepted structure consists in carbonyl and carboxyl groups located at the edge of the graphene network and hydroxyl and epoxy groups attached to the basal plane. The percentage of O-groups depends on the synthesis route and the material used as carbon source. In addition, highly oxidized fragments, called oxidative debris, OD, are produced during the oxidation process. These fragments are adsorbed onto the graphene oxide network and can be removed by alkaline washing. The purified material has lower O/C ratio than graphene oxide and its properties are also quite different. Due to its structure, graphene oxide can be adsorbed at the air-water interface of the aqueous solution by diffusion, Gibbs monolayers, or by spreading on a clean water subphase resulting in a Langmuir film. This review is intended to provide information on the importance of controlling the chemical composition, structure, size, and oxidative debris, on the manufacture of graphene oxide films. To this end the review shows the influence of the synthesis route and the starting material on the structure of graphene oxide and analyzes several examples of the behavior and properties of films prepared with different types of graphene oxides. The great variability of behaviors of graphene oxide films caused by the different structure of this material provides a great opportunity to fine-tune the properties of films according to the needs of different applications.

Contents

1. Introduction

Graphene Oxide (GO) is a carbon-based nanomaterial obtained by the chemical oxidation of natural graphite or carbon nanofibers by strong oxidants. This material was known much before pristine graphene [1] and it is considered as one of the most important materials precursors of graphene [2]. Due to the presence of oxygen functional groups, GO must be reduced by thermal [3] or chemical procedures [4] to obtain graphene. However, these procedures do not completely restore the structure of graphene and some O-groups remain attached at the basal plane modifying the properties of graphene oxide [5,6]. This new material, referred as reduced graphene oxide, rGO, can be used as component of conductive electrodes [7], light emitting diodes

* Corresponding author.
E-mail address: mvsal@usal.es (M.M. Velázquez).
[1]Present address: Departamento de Química Analítica, Química Física e Ingeniería Química, Universidad de Alcalá. 28,871 Alcalá de Henares, Madrid, Spain.

https://doi.org/10.1016/j.cis.2020.102312
0001-8686/

[8], and photovoltaic cells [8,9]. In applications such as biosensing [10,11], design of inks [12], drug delivery vectors [13] or bioimaging [14], graphene oxide presents several advantages because the oxygen groups can bind polymers, nanoparticles or other molecules to tune the properties of new materials according to the needs of the different applications. Furthermore, the O-groups provide aqueous dispersibility to graphene oxide, which is an important property in biomedical applications [15–17].

An interesting property of graphene oxide is that it can behave as a surfactant due to its ability to adsorb at the air-water interface [18,19]. This behavior can be interpreted by the existence of hydrophilic moieties such as carboxyl, epoxy or hydroxyl groups and a more hydrophobic region constituted by the hexagonal carbon network. Due to this feature, graphene oxide has been widely used to stabilize oil-water emulsions [19–23], Pickering emulsions [24–30] or miniemulsions [31], and as a foam stabilizer agent [32]. Recent works have investigated the effect of pH, GO size and concentration on the adsorption dynamics [33,34] and mechanical properties [34] of GO films at the water-oil interfaces. However, it is still controversial to consider graphene oxide as a conventional surfactant, since one of the most salient properties of surfactant molecules is the ability to form micelles and that ability has not yet been reported for graphene oxide [35]. It is possible to find abundant literature stating that GO behaves as a surfactant [18,19,36,37] due to its ability to locate at the interfaces. However, other works analyze its behavior as particle since it stabilizes different types of emulsions [20,23,29,30] or form liquid crystals in concentrated solutions due to the preferential alignment of GO sheets [38,39]. A recent review discusses the possible reasons for this dual behavior [40].

Much of the studies on the surface activity of graphene oxide have been focused on the effect of pH and ionic strength. As in some surfactant molecules [41,42], the surface activity of GO depends on the pH of the solutions as well as the ionic strength [43]. Therefore, the ability to stabilize emulsions also depends on both, the pH [44] and the presence of electrolytes in the solution [45]. This behavior was discussed in terms of the existence of carboxyl groups at the edges of the sheets which can be protonated or deprotonated by changing the pH of the solution. Thus, in acidic medium, pH < 1, the acidic functionalities protonate, and graphene oxide becomes more hydrophobic, while when the pH increases, graphene oxide sheets retain the negative charge and are stable in aqueous solutions [44]. However, not only the properties of the medium, such as pH or ionic strength, can modify the surface activity of graphene oxide, but also structural properties such as size and oxidation degree affect its adsorption capacity at the interfaces. The amphiphilicity of GO has been shown to depend on the size of the sheets [43]. Besides, the reduced graphene oxide is more hydrophobic than graphene oxide due to its lower percentage of O-groups and consequently, presents a higher affinity for hydrophobic phases than graphene oxide [36]. However, there is a significant lack of knowledge about the effect of the graphene oxide structure on its surface activity. This is especially important considering that the GO structure and the degree of oxidation are influenced by the oxidation route, and the starting material. Therefore, it is crucial to analyze how the chemical and structural variability of graphene oxide can influence its surface activity. A deep study is specially required for applications in which GO must be adsorbed at the interfaces. On the other hand, the structural variability of GO could be the origin of the diverse surface behaviors reported in the literature.

This review focuses on unraveling the complexity of the interfacial adsorption properties of GO by analyzing the role of the structure and chemical composition in the surface activity of graphene oxide. The work is organized as follows: firstly, the synthesis routes and the chemical structure of graphene oxides will be summarized, paying attention to the dependence of the chemical structure on the synthesis route and the starting material. In the next section, we will discuss the surface activity of graphene oxide dispersions and the surface properties of Langmuir films of different graphene oxides. At the end of that section, we analyze the role of oxidative impurities, referred as oxidative debris (OD), in the organization of graphene oxides films studied by neutron reflectivity.

2. Graphene oxide synthesis and structure

2.1. Synthesis of graphene oxide

The first synthesis of graphene oxide was done by Brodie [1] in 1859. He used a mixture of graphite and fuming nitric acid in the presence of potassium perchlorate at 60 °C for three or four days. The material thus obtained was washed and the oxidation process was repeated four times and finally the solid was dried at 100 °C. The C:H:O ratio of the light-yellow solid thus obtained was: 61.04: 1.85: 37.11. The solid material disperses in water or basic aqueous solutions and Brodie named it as graphic acid.

Staudenmaier improved the synthesis procedure [46] by adding small among of potassium perchlorate and acidifying with sulfuric acid. The procedure leads to the same C/O ratio as that obtained by Brodie but avoids the repetitive oxidation. A few years later, the fuming nitric acid was replaced by non-fuming nitric acid by Hofmann [47] and in 1958 Hummers and Offeman [48] replaced nitric acid by potassium permanganate as oxidant and a mixture of concentrated sulfuric acid and sodium nitrate. This method produces nitric acid *in situ* and is one of the most widely used today.

To avoid the production of the toxic gases, NO_2 and N_2O_4, Tour [49,50] replaced the sodium nitrate by phosphoric acid. The authors state that this procedure leads to more oxidized GO than the Hummers' method and the basal plane also remains more intact. These methods have been used interchangeably for years assuming that the properties of GO are almost the same. However, when graphene oxides were characterized by X-ray photoelectron spectroscopy (XPS), Fourier transform infrared (FTIR), and Raman spectroscopies and electrochemical techniques, the results showed a large disparity between the oxygen functionalities, and the electron-transfer rates [51]. These facts showed large differences between graphene oxides obtained by different oxidation routes.

In all these methods the starting material was graphite; however, we recently reported that the chemical composition, surface charge density, and size of the graphene oxide sheets can be tuned using the same synthesis method, the Hummer's procedure, but modifying the starting material [52]. Accordingly, the starting material and the oxidation route must be chosen to obtain the graphene oxide adapted to the needs of each application.

2.2. Graphene oxide structure

Although the synthesis of GO has been known for more than 100 years, its structure is still under debate. This is because its stoichiometry depends on the type of starting material [52] and the oxidation protocol [53,54].

The structure of graphene oxide is made up of graphene sheets with several oxygen groups attached at the basal plane. ^{13}C and ^{1}H magic angle spinning nuclear magnetic resonance (MAS NMR) [55–57] and X-ray photoelectron spectroscopy (XPS) studies [57,58] identified these O-groups as hydroxyl, carbonyl, epoxy, and carboxyl groups. The most accepted model was proposed by Lerf and Klinowski [55–57] and considers the carboxyl and ketone groups are mainly located at the edges of sheets, while the 1.2 epoxy and hydroxyl groups are found attached to the basal plane, Fig. 1. Recent scanning transmission X-ray microscopy (STXM) and high-resolution near-edge X-ray absorption fine structure (NEXAFS) spectroscopy experiments have confirmed the GO structure proposed by Lerf and Klinowski.

Recently, the structure of graphene oxide was revisited since it was proved that the oxidation of graphite, nanotubes and other carbonaceous materials originates highly oxidized organic fragments referred

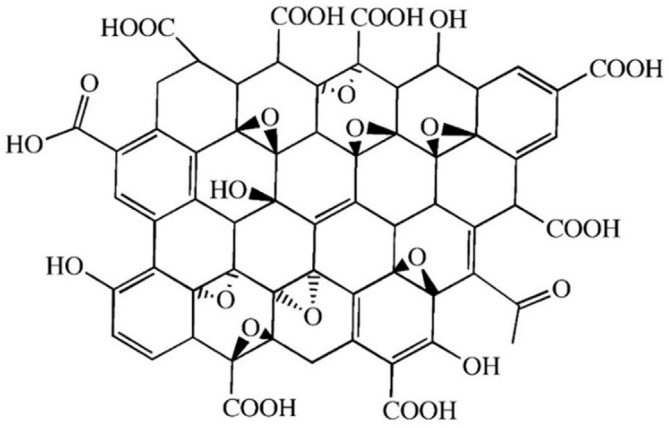

Fig. 1. Graphene oxide structure according to the Lerf and Klinoswki model [57].

to as oxidative debris (OD). The OD composition found by high-resolution mass spectrometry [59] was $C_{19}H_{35}O_6$ and $C_{18}H_{33}O_9$ (1,1). These highly oxidized fragments are adsorbed on graphene oxide sheets through π-π stacking [16] and are removed by alkaline washing, Fig. 2.

Graphene oxide purified by alkaline washing has lower amount of oxygenated groups than the non-purified material, and exhibits a quite different structure and properties [52,60–62]. It has been demonstrated that the OD adsorbed on the GO sheets decreases the electric conductivity around five orders of magnitude [59] and increases the water dispersibility of GO. Besides, OD also modify the spectroscopic properties of graphene oxide [63]. An example is the absorption of UV–Vis light, Fig. 2. The main feature of the absorption UV–Vis spectrum of GO is an intense band at 228 nm, characteristic of the transition $\pi \rightarrow \pi^*$ and a shoulder around 300 nm attributed to the $n \rightarrow \pi^*$ electronic transition of C═O bonds [64,65]. After alkaline washing, the band centered at 228 nm is red shifted to 250 nm, Fig. 2, due to the restoration of the sp^2 conjugation [64,65] produced by removing the highly oxidized fragments of OD. This behavior is easily visualized by the different color of the dispersions, light brown for graphene oxide and grey for purified graphene oxide, Fig. 2. The Photoluminescence properties are also quite different for these two materials. The purified material does not emit fluorescence [66], while GO presents an important blue emission assigned to OD [67,68]. As will be shown later, the surface properties of purified and unpurified graphene oxides are also quite different.

Starting from the oxidation by the Hummer's method slightly modified [5] and using five different starting materials combining with the alkaline washing, we have synthesized ten different graphene oxides with distinct chemical composition, size, surface charge and structural defects [48]. Therefore, we think that this strategy can be used to tune the structure of GO according to the needs of each application.

Another structural aspect which modifies the mechanical, chemical and electronic properties of graphene oxide is the presence of defects in the basal plane [69,70]. Defects are categorized as intrinsic and extrinsic. The intrinsic defects are caused by the existence of some non-hexagonal rings, referred as vacancies, or by line defects referred as grain boundary. The extrinsic defects in graphene oxide correspond to O-groups attached to the basal plane. Therefore, it is crucial to identify and quantify the different types of defects.

Defect identification can be carried out by Raman spectroscopy since the phonon modes provide information about them. Works carried out by different groups [71–78] have shown that the Raman spectrum of graphene presents two prominent bands centered at 1582 cm^{-1} (G band) and at 2700 cm^{-1} (2D band) band, see Fig. 3a; but, when defects on the periodic lattice of graphene appear, two new bands, referred as D (1350 cm^{-1}) and D' (1626 cm^{-1}), also appear. As can be seen in Fig. 3b these two new bands are also in the Raman spectrum of graphene oxide, indicating the existence of defects.

However, despite the Raman spectrum of graphene is currently understood, the Raman spectrum of GO is controversial, due to the great variability of experimental results referred to the position and the width of some peaks and the attribution of the new bands [79,80]. On the other hand, *ab initio* calculations [81,82], used to simulate the Raman spectrum of GO, showed that the intensity and width of some Raman peaks and the appearance of new bands are related to the local atomic configuration. Therefore, we think that to interpret the Raman spectrum of GO a systematic study of the evolution of the Raman spectrum of GO with the chemical composition and structural defects is necessary. We recorded the Raman spectra of the graphene oxides synthesized with different starting materials and using the alkaline

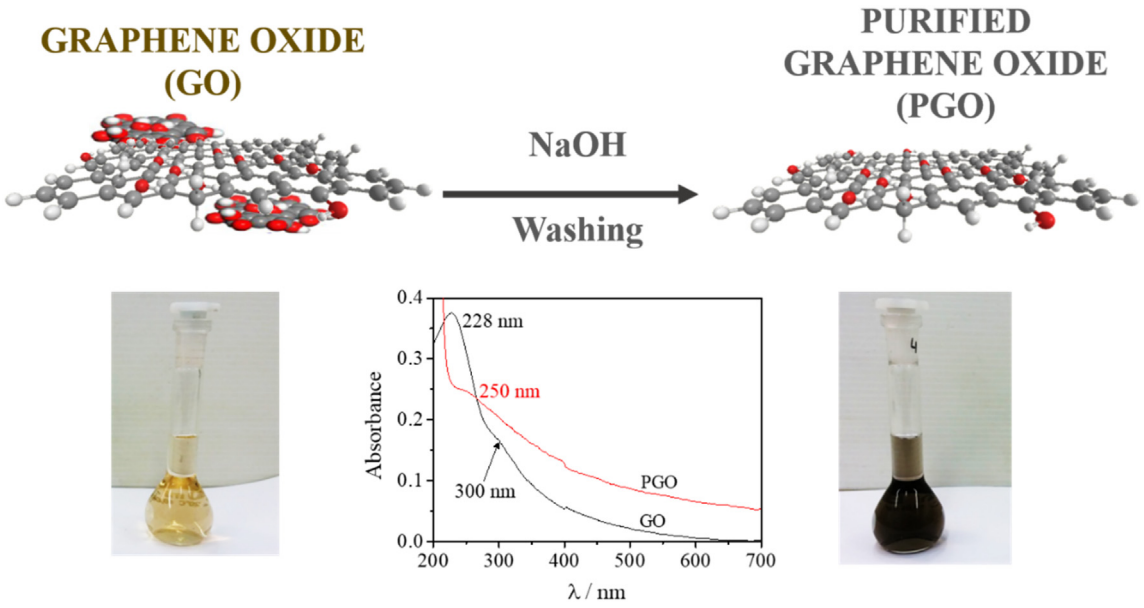

Fig. 2. The scheme shows the process of purification by alkaline washing of graphene oxide. Photographs of 0.1 mg/ml solutions of graphene oxide and purified graphene oxide (OD free). UV–Vis spectrum of aqueous solutions of: GO (0.012 mg/ml) and PGO (0.0051 mg/ml).

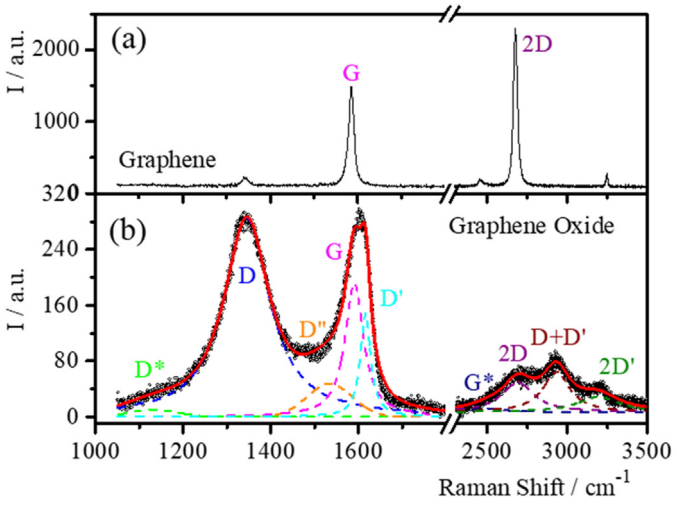

Fig. 3. Raman spectra of (a) graphene and graphene oxide (b). Graphene was obtained by exfoliation of graphite flakes and graphene oxide was synthesized by oxidation of graphite flakes. Dashed lines in (b) are the functions into which we split the experimental spectrum (circles), and the solid line represents the fit to the experimental data.

washing as purification procedure; the results allowed us to correlate the relative intensity, the position and the width of the band with the percentage of different O-groups determined by XPS and with structural defects, respectively [52].

All the graphene oxide Raman spectra showed D and G bands at 1350 and 1585 cm^{-1} and three bands corresponding to the second-order spectrum above 2600 cm^{-1}. We also detected new bands centered at 1610 cm^{-1} (D' band), 1530 cm^{-1} (D" band), and 1150 cm^{-1} (D* band), see Fig. 3b. It is well established that D and D' bands appear when defects break the periodic lattice of graphene [83]. However, in the case of the Raman spectrum of GO, there is lack of acknowledgement of the type of defects involved. On the other hand, to interpret correctly the origin of D" and D* bands in graphene oxide, we used organic elemental analysis and X-ray diffraction measurements apart of the Raman spectroscopy [6]. We were able to relate the D" band with the crystallinity of the material [84] and the D* band with the disorder of the graphitic lattice due to the existence of sp^3 bonds [85–87].

Three bands centered at 2690, 2930, and 3190 cm^{-1}, constitute the second order spectrum. The band centered at 2690 cm^{-1} is unequivocally ascribed to the 2D band [77]. However, there were some controversies in the assignment of the two other bands. To assign these bands we compare the frequencies of the 2D, the combination of bands D + D' and 2 D' band with twice the frequency of band D, the sum of the frequencies of bands D and D' and twice the frequency of the D' band, respectively and the values agreed very well. These facts made it possible to unambiguously assign these peaks to the bands 2D, D + D', and 2D' bands, respectively [52]. In Fig. 3b is possible to see a weak band around 2500 cm^{-1}. This peak named as G* has been shown in other Raman spectra of graphene oxides and is due to an intervalley process involving one inplane transverse optical (iTO) phonon and one longitudinal acoustic (LA) phonon [86]. We observed that the peak is shifted 35 cm^{-1} to higher wavenumber values in the Raman spectra of purified graphene oxides.

We have found correlations between the intensity and the position of the D* band and the oxidation degree of graphene oxide [6]. Besides, we found linear correlations between the I_D/I_G ratio, the positions of the 2D and D + D' bands and the percentage of Csp^2 determined by XPS [52] as well. We have also interpreted the changes in the relative intensity of D' and D bands with the type of structural defects according to the double-resonance mechanism [88]. This model was proposed to interpret the Raman spectrum of defective graphene. The model relates the relative intensity values of bands D' and D with grain boundaries, vacancies and sp^3 hybridization defects, respectively. Our results showed that vacancy-like defects predominate in large GO sheets (diameter > 400 nm) while sp^3 hybridization defects predominate when the sheet diameter is around 100 nm [52]. Finally, grain boundary defects were observed for GO sheets synthesized by carbon nanofibers and subsequently annealed between 100 and 800 °C [89]. Recently, we have used these correlations to analyze the effect of thermal annealing on the structure of GO inserted between hexagonal boron nitride flakes [89].

3. Graphene oxide trapped at the air-water interface

Due to its structure, graphene oxide can be trapped at the interfaces. However, its behavior at the interfaces is quite different to that of conventional surfactants. In this section, we analyze results reported in the literature referred to the ability of GO to adsorb at the air-water interface of water dispersions and the structure and properties of Langmuir films of graphene oxide.

3.1. Surface activity of graphene oxide water dispersions

The stability of graphene oxide in water is attributed to the electric charge produced by the ionizable groups attached to sheets. Three pK values for graphene oxide have been reported: 4.3, 6.6, and 9.8 [90]. They were assigned to carboxyl groups close to the hydroxyl groups (4.3), carboxyl (6.6), and phenolic groups (9.8), respectively.

We analyze the variation of surface electric charge of graphene oxide and purified graphene oxide with pH in Fig. 4. The results of Fig. 4 correspond to graphene oxide synthesized from graphite flakes, referred as GO and to purified graphene oxide, called PGO, obtained by washing GO in an alkaline medium. The C/O ratio are 1.6 and 4.3 for GO and PGO, respectively [91]. As can be seen in Fig. 4, the GO sheets wear negative electric charge even at pH = 1. It was no possible to work at pH < 1 because GO sheets aggregate [44]. The results also show that the zeta potential of PGO solutions are lower than for GO. This behavior can be interpreted by considering that when OD are removed by alkaline washing, many O-groups are also removed, and the zeta potential decreases compared to the non-purified material.

The stability of sheets in aqueous solutions also depends on the GO concentration. Graphene oxide is stable even at concentrations of 60 mg/ml, while reduced graphene oxide is stable at concentration values below 0.5 mg/ml [64,92]. Rheological studies showed the existence of

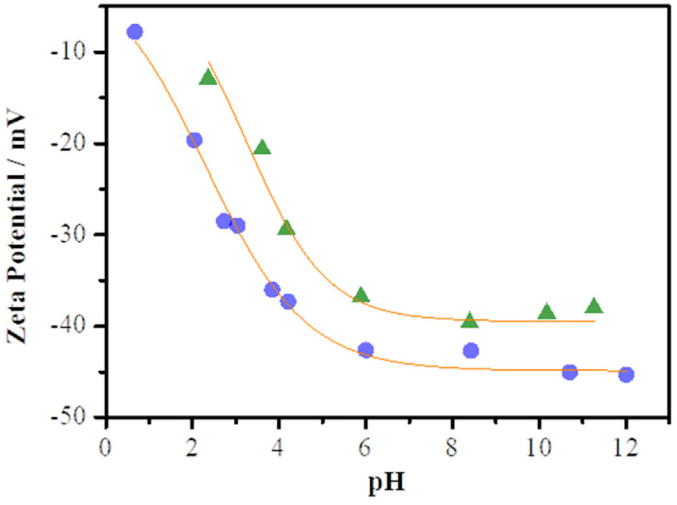

Fig. 4. Variation of the zeta potential with pH: GO (circles) and PGO (triangles). Measurements were done at 293 K. The solution concentrations were 0.12 mg/ml. Lines are just visual guides.

a critical concentration [93] below which GO sheets are dispersed and above which they aggregate or dismantle depending on whether a Brownian diffusion mechanism or convective flows predominate [94]. The transition between dispersed sheets and aggregates is similar to isotropic-nematic liquid crystal transitions [95]. Furthermore, the concentrated dispersions behave as thixotropic materials [95]. These results do not evidence micelle formation in concentrated GO dispersions; however, there are several experimental evidences for the formation of highly ordered self-assembled nematic crystal liquids above 10 mg/ml [96]. Other 2D systems such as graphene or molybdenum disulfide sheets present the same behavior [97]. The formation of nematic crystal liquids in highly concentrated GO solutions was attributed to attractive interactions between sheets through π-π staking [96,98]. Some works reported that GO sheets in the nematic structure are fully extended [99]; however, recent neutron scattering measurements showed a scattering pattern compatible with crumpled structures [100]. The high flexibility of graphene oxide sheets favors the interactions between the hydrophobic domains and could be responsible of crumpling.

The ability of GO to adsorb at the interfaces from solutions is due to its amphiphilic character. Since graphene oxide presents carboxyl groups at the edge of sheets, the difference between the hydrophilicity of the O-groups and the hydrophobicity of the aromatic domains can be tuned by changing the pH. Accordingly, one expects that at high pH values, the GO behaves like a surfactant molecule with affinity by the air-water interfaces, since the carboxyl groups are deprotonated. However, surface tension measurements at pH of 14 and 1 showed that at pH = 14 the surface tension is independent on the GO concentration and it remains constant at the value of the pure water (72.8 mN/m). Nevertheless, at pH = 1, the surface tension of the GO solutions decreases until 52 mN/m when the GO concentration reaches a value of 1 mg/ml. This means that GO behaves as a surfactant at pH = 1 [44], while at high pH remains stable in aqueous solutions. The cause of this behavior is the great hydrophilicity of sheets in alkaline medium due to the deprotonation of the carboxyl and phenolic groups at the edges of the sheets [44]. To increase the adsorption of GO at the air-water interface, Kim et al. proposed a method consistent in bubbling gas in the GO solutions [18]. They suggest that the diffusion of GO sheets from bulk to the interface is very slow due to the large dimensions of sheets; therefore, the bubbling procedure accelerates the diffusion process.

Apart from the pH, the amphiphilic character of the GO sheets can also be modified by changing the size, oxidation degree, and purity. Smaller sheets have been shown to be more hydrophilic than large sheets because they contain more O-groups at the basal plane [43] and have a higher superficial charge density [52]. Conversely, the sheets of reduced graphene oxides are more hydrophobic than the graphene oxide sheets, since they have lower charge density at the edges [36]. Therefore, it is expected that the ability of graphene oxide to be transferred from the aqueous solutions to the air-liquid interface can be adjusted by changing the structure of sheets. However, the mechanism of adsorption of GO is still an object of study. Thus, in a recent work the effect of a cycling pH on the GO surface coverage was studied [43]. Results show that GO is only surface active in acidic aqueous subphase, but when the pH of the aqueous subphase increases, most of the GO sheets remain trapped at the interface. This behavior is quite different to that observed in the case of surfactant molecules adsorbed at the air-water interface and was attributed to the high values of desorption energy (10^5–10^7 kT) [101] compared to the values corresponding to the anionic surfactants. Besides, the larger size of GO sheets compared with conventional surfactant molecules makes the desorption slower than that of surfactant molecules, improving its stability at the interface [20]. Consequently, to achieve high GO coverages, it is necessary to simultaneously consider the structural aspects that can modify the amphipathic character of GO sheets and the thermodynamic aspect of the desorption process of the sheets trapped at the interface.

3.2. Langmuir films of graphene oxide

Another way of trapping graphene oxide sheets at the air-water interface is across the manufacture of Langmuir monolayers. Monolayers of surfactant agents floating at the air-water interface are referred as Langmuir monolayers and are prepared by dissolving amphiphilic molecules or nanoparticles in a volatile organic solvent, typically chloroform, and then placing a small volume of the spreading solution on a clean water surface using a Langmuir-Blodgett trough. After the solvent evaporation, the amphiphilic molecules remain irreversibly pinned at the interface. The intermolecular distance can be modified by symmetrical compression with two barriers. Different degrees of compression can lead to phase transitions between gaseous, liquid, and solid surface states, and can eventually lead to collapse in multilayers, [102,103]. In the case of graphene oxide, stable Langmuir monolayers have been reported by spreading GO sheets dissolved in methanol/water mixtures on acidic aqueous subphases [5,18,19,36,91,104–106].

To study the influence of the chemical composition of the different types of graphene oxide on the surface states of the monolayers, we prepared Langmuir monolayers of different graphene oxides synthesized by the oxidation of graphite flakes and the carbon nanofibers GANF®, and purifying these graphene oxides by alkaline washing [91,105]. The C/O ratios of these materials ranged from 1.6 to 4.3 [52]. Fig. 5 shows the surface pressure, π and compressional elastic modulus, C_s^{-1}, *versus* the surface area, A, isotherms of graphene oxide obtained from graphite flakes GO and purified graphene oxide PGO, respectively [91,105,106]. Similar results were obtained for graphene oxides obtained from carbon nanofibers. The surface compressional elastic modulus was calculated from the surface pressure isotherms by using the following equation: $C_s^{-1} = -A\left(\frac{\delta\pi}{\delta A}\right)_{p,T}$.

To deepen the morphology of the different surface states, different authors obtained Brewster Angle Microscopy (BAM), Atomic Force Microscopy (AFM) and Scanning Electron Microscopy (SEM) images of monolayers at different surface states [91,104]. Fig. 6 shows a SEM image of graphene oxide synthesized from graphite and deposited by the Langmuir-Blodgett methodology at 4 mN/m.

It was demonstrated that the monolayers at surface pressure and compressional modulus close to zero, present a density of sheets too low to be observed by BAM. This behavior is consistent with isolated GO sheets [37,91]. As the surface pressure increases, BAM images show the GO sheets approach each other and both, the surface pressure, and the compressional elastic modulus increase [91]. AFM and SEM images of films transferred onto a solid showed that the distance between sheets is very small in this surface state referred as close-packed region [104]. When the GO film is further compressed, the surface pressure slightly increases. SEM images obtained by other authors showed folded sheets at the contact points [104].

As can be seen in Fig. 5c and d, at higher surface pressure values (30–40 mN m^{-1}), the compressional elastic modulus presents two different behaviors. In the non-purified GO films, the compressional elastic modulus decreases, while in films of purified graphene oxide, the compressional elastic modulus increases and goes through a maximum [91,106]. The decrease of the compressional elastic modulus is attributed to the collapse [104] and as show results in Fig. 5c and d, the two monolayers collapse; however, in the isotherms of the purified material, prior the collapse, the surface pressure and the compressional elastic modulus increase with compression. This region has been assigned to a dense monolayer of interlocked GO sheets with wrinkles [104]. This interlocked region drives to the collapse after further compression. The differences observed between the monolayers of purified and non-purified graphene oxides are due to the presence of oxidative debris, OD as discussed below.

To describe the isotherms of graphene oxides trapped at the air-water interface, we used a model derived by Miller's group [107]. The model is based on another one proposed to describe the behavior of

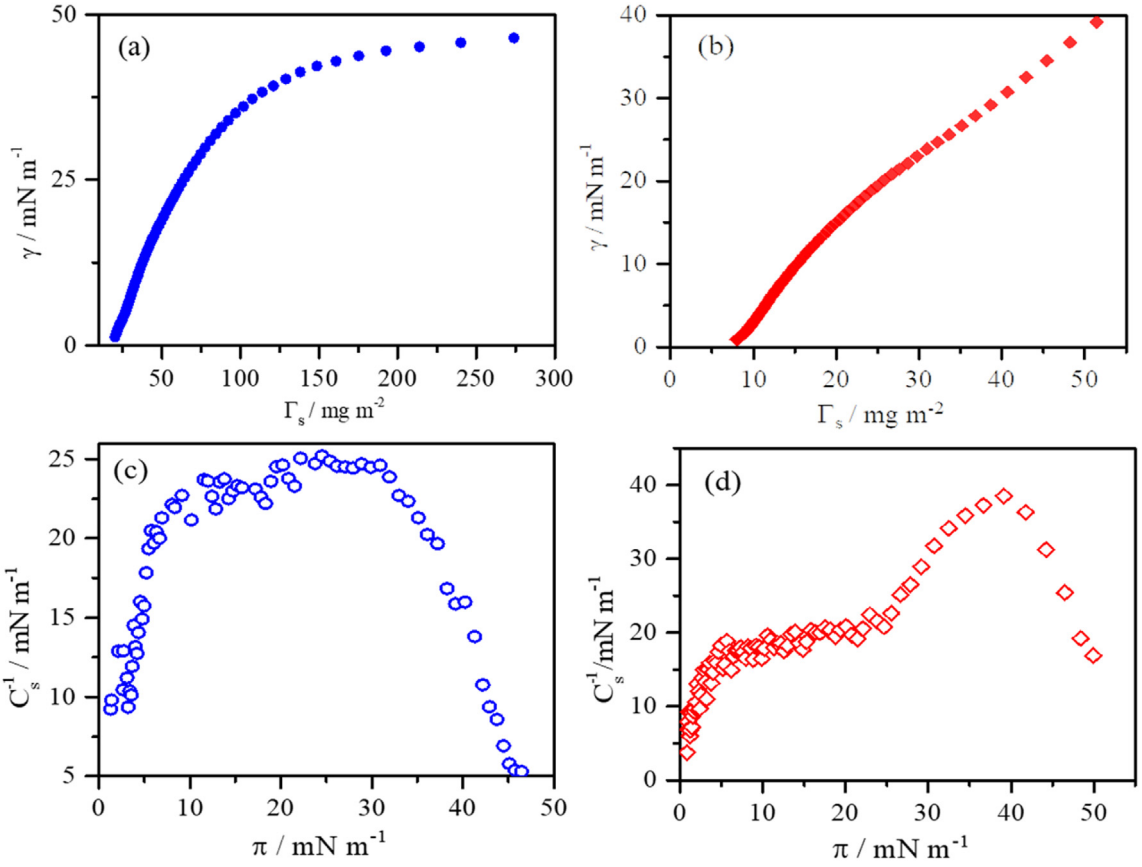

Fig. 5. Surface pressure isotherms of GO (a) and PGO (b). The isotherms are recorded at 293 K. (c) Surface compressional elastic modulus isotherms of GO (c) and PGO (d). Reprinted with permission from Ref. [106]. Copyright (2020) American Chemical Society.

proteins at fluid interfaces [108], generalized for nanoparticles and used by Imperiali et al. [101] to describe GO isotherms. For a Langmuir monolayer, assuming interactions between nanoparticles, the state equation is [107]:

$$\Pi = \frac{kT(\omega/A)}{\omega_0[1-(\omega/A)]} - \Pi_{coh} \quad (1)$$

In Eq. (1) ω and ω_0 represent the total surface area occupied by graphene oxide sheets and by water molecules, respectively. Π_{coh}, is the surface pressure cohesion and k and T are the Boltzmann constant and the absolute temperature. The surface pressure cohesion includes the contributions to surface pressure from all interactions within the surface, solvent-solvent, solvent-solute and solute-solute.

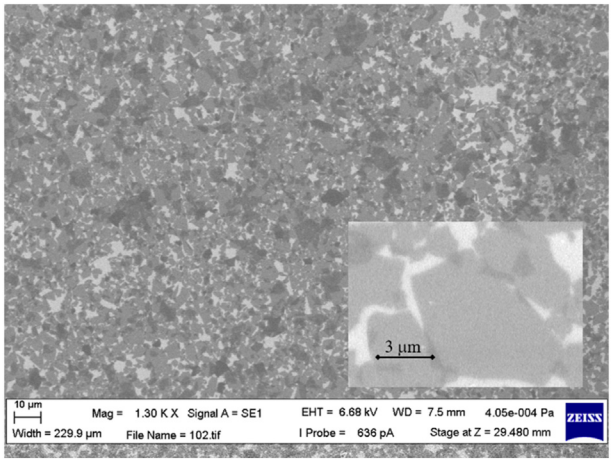

Fig. 6. SEM image of a graphene oxide film prepared by the Langmuir-Blodgett methodology. The inset is a magnification to show the morphology of sheets.

In Fig. 7, the experimental surface pressure values corresponding to NGO and PNGO are plotted against the trough area and lines are calculated from Eq. (1). As can be seen, the model interprets acceptably the experimental values in the close-packed region [87,101], however, it fails outside the closed-packed region, Fig. 7. This behavior has been reported by Imperiali [101] who considered that the model was proposed to describe particle films in the liquid expanded state [103]. Therefore, in the case of graphene oxide films, it should be used in the region where there is no deformation in the film caused by wrinkles or platelet overlapping [97], *i.e.* the closed-packed region. Results plotted in Fig. 7 correspond to monolayers of purified and non-purified graphene oxide synthesized from carbon nanofibers GANF®, but the same behavior was observed for graphene oxides obtained by oxidation of graphite flakes [105].

The cohesion pressure parameter values obtained from fits, Fig. 8a, are positive and linearly correlate with the percentage of carboxyl groups attached at the basal plane of graphene oxide [105]. The positive value of the cohesion pressure parameter indicates the existence of net attractive forces between sheets. It is well established that capillary forces and line tension can contribute together with specific interactions to the lateral attractive interactions between sheets. However, it has been shown that the magnitude of capillary and line tension forces is not very large [101], so that, specific interactions constitute the main contribution to the value of the cohesion parameter. We consider that attractive interactions between carboxyl groups through hydrogen bonds [109] may be an important contribution to the cohesion pressure parameter. Therefore, we analyze the effect of pH on the cohesion

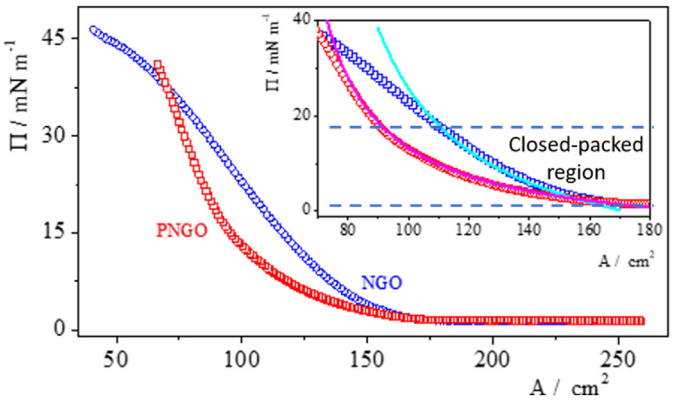

Fig. 7. Pressure surface-area isotherms of NGO (circles) and PNGO (squares) recorded at 293 K. Lines are calculated according to Eq. (1). Adapted with permission from Ref. [91]. Copyright (2013) Wiley-VCH Verlag GmbH & Co. KGaA, Weinheim. Dashed lines mark off the closed-packed region.

pressure [105], Fig. 8b. The results show that the highest values of cohesion pressure are observed for monolayers deposited on acidic aqueous subphases, pH < 3, where the carboxyl groups are protonated [105]. Consequently, the formation of hydrogen bonds between carboxyl groups attached to the sheets [109] seems to be one of the most important contribution to the surface pressure cohesion parameter.

We also found a correlation between the cohesion pressure parameter and the sheet packing of in the closed-packed region. In Fig. 8c the cohesion pressure parameter values are plotted against the surface compressional modulus taken at the end of the closed-packed region. As can be seen in Fig. 8c the cohesion pressure parameter linearly depends on the compressional elasticity modulus. To interpret this behavior, it is necessary to consider that, according to our results, the most important contribution to the cohesion pressure parameter is the formation of hydrogen bonds between carboxyl groups attached to the sheets [109]. Therefore, when attractive interactions increase, which means high Π_{coh} values, the GO sheets are strongly packed through the hydrogen bonds and the compressional elasticity modulus increases as well.

3.3. Effect of oxidative debris on the structure of Langmuir films of graphene oxide

As mentioned above, the oxidation of graphite or other carbonaceous materials results in the formation of oxidative debris, OD. This oxidative debris is adsorbed on the graphene networks modifying its

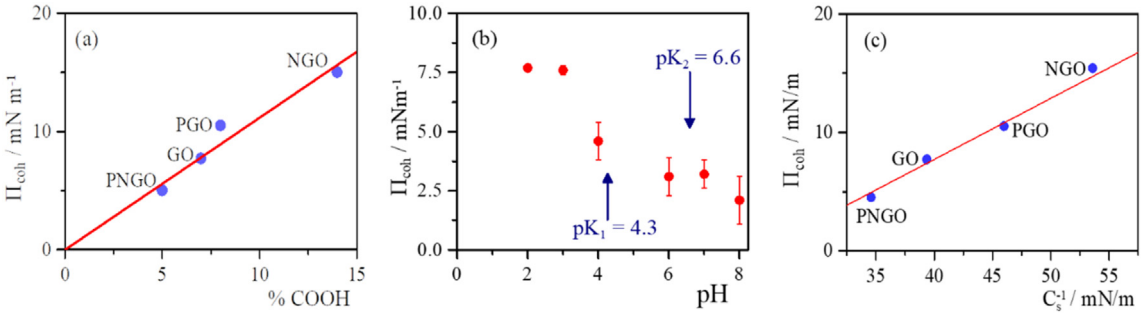

Fig. 8. (a) Variation of the cohesion pressure parameter with the percentage of COOH obtained by XPS measurements. (b) Variation of the cohesion pressure with pH. Data correspond to graphene oxide obtained by oxidation of graphite flakes, GO. Adapted with permission from Ref. [105]. Copyright (2015) American Chemical Society. (c) Variation of the cohesion pressure parameter with the compressional elasticity modulus of the closed-packed region. The cohesion pressure parameter values were taken from ref. [105].

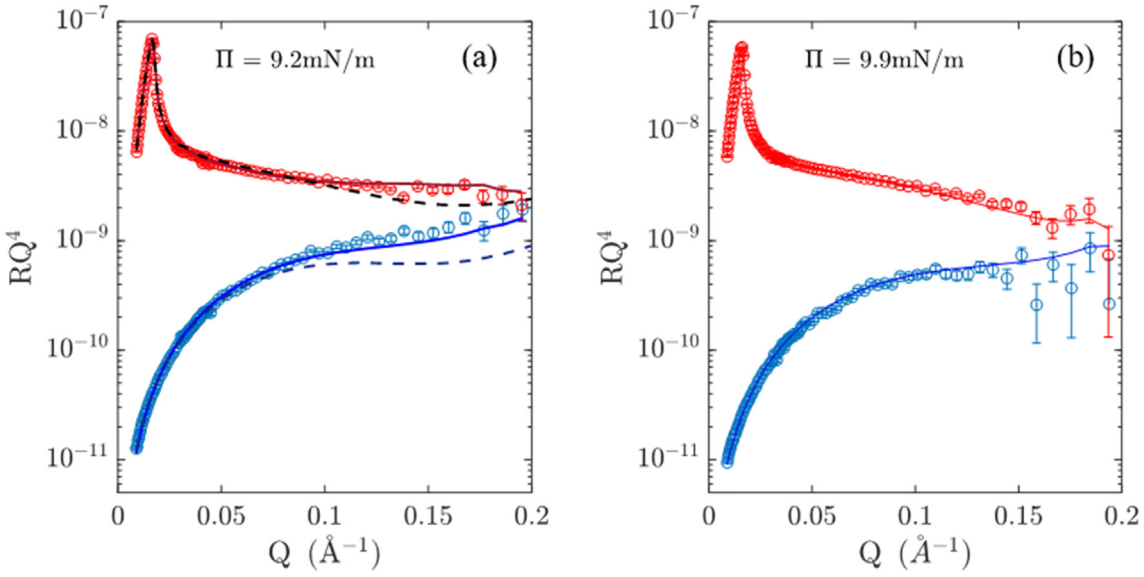

Fig. 9. Experimental reflectivity profiles (symbols) and simulated (lines) values calculated according to a 2-layer model for GO films (a) and one layer for PGO (b). In Fig. 9(a) the dashed line is the simulated line calculated from a single layer model. Red symbols and lines correspond to measurements in pure D_2O contrast and symbols and lines in blue to ACMW contrast (mixture of 8.1% *v*/v D_2O: H_2O). Adapted with permission from Ref. [106]. Copyright (2020) American Chemical Society.

properties. The effect of OD on the properties of graphene oxide in bulk is well known and was previously commented, but there is little information about the role of OD on the properties and structure of graphene oxide films trapped at interfaces. However, we think that the organization of OD at the interfaces, and its effect on the surface properties of films are crucial in those applications where graphene oxide is adsorbed at the interfaces. Therefore, we use neutron reflectivity measurements to study the effect of OD on the structure of graphene oxide films.

Specular neutron reflectivity (SNR) is a suitable technique to study the structure of different systems trapped on fluids interfaces [110,111], therefore, we used SNR to analyze the role of OD in the structure and properties of graphene oxide at the air-water interface. This technique was previously used to evaluate the adsorption of different organic solvents on GO films deposited onto silicon [112,113], but, as far as we know, it has not been used to study the structure of GO sheets at the air-water interface. Recently, measurements of X-ray reflectivity (XRR) and grazing incidence X-ray diffraction (GIXD) were used to study GO films at the air-water interface. The results show that the graphene oxide films are constituted by a bilayer of GO sheets whose thickness and roughness evolve with the surface density [114]. To deepen the effect of the OD on the structure of GO Langmuir films, SNR measurements of purified (OD free) and non-purified graphene oxide Langmuir films were recorded at two surface pressure values into the closed-packed region. Our results show significant differences between the film structure of these two materials [106]. Thus, the reflectivity profile of GO films is satisfactory interpreted with a bilayer model, in agreement with X-ray surface scattering results previously reported [114]. The bilayer is made up of 2–3 graphene oxide layers in contact with air and a second layer submerged in the aqueous subphase. When the OD layer was removed by alkaline washing, purified graphene oxide, the film is exclusively composed by the single layer of GO. Our results allow us to demonstrate that the second layer is constituted by OD. Illustrative examples of the two different behaviors can be seen in the reflectivity profiles collected in Fig. 9.

It is worth noting that the roughness of the GO and PGO layers in contact with air far exceed the value originated exclusively by capillary waves (3.1 Å). This fact points to the existence of additional roughness probably caused by protrusions at the interface. These protrusions evolve as the molecular area decreases [106].

The existence of a second layer of highly oxidized molecules, OD, in the GO films may explain the different behavior observed for the compressional elastic modulus at the isotherms of GO and PGO. As discussed above, PGO film collapses at higher surface pressure than GO film and, before the collapse, presents higher compressional elastic modulus values than the GO film (Fig. 5c and d). To interpret this behavior it is necessary to consider that since the OD fragments are formed by highly oxidized molecules adsorbed onto graphene oxide network, GO is more hydrophilic than PGO, consequently, it collapses by expulsion at low surface pressure values [115]. In contrast, the most hydrophobic material, PGO, is subjected to stronger cohesive forces than GO and goes through a surface solid state of high compressional elasticity modulus prior the collapse.

4. Summary and outlook

This review summarizes the great variety of sizes, chemical composition, polydispersity degree, surface electric charge of graphene oxide, obtained by different synthesis routes and starting materials. This variability makes possible to design materials according to the needs of each application by selecting the synthesis procedure or the starting material. This is especially important in the manufacture of sensors, biosensors, catalysts, or hybrid materials in which the type of functional group, electric charge or the size of sheets are crucial.

We also analyze the influence of some structural characteristics of graphene oxides on the properties of graphene oxide films at the air-water interface and we show the complex behavior of this material at the interface. We show the possibility of improving the surface density of graphene oxide films by decreasing the pH or by increasing the O-groups attached at the basal plane. On the other hand, our results show that the oxidative impurities, constituted by highly oxidized molecules, form a second layer at the interface submerged in water. This second layer increases the surface density and decreases the elasticity of the films compared with films of the purified material. This behavior should be considered in some applications where graphene oxide acts as a stabilizing agent of foam, emulsions, or Pickering emulsions.

Despite all this information, there are still several aspects to explore. It is necessary to study the effect of the number of GO layers on the organization of the films and the effect of the structure and chemical composition of GO on the dynamic of adsorption and on the rheological properties of the GO films. On the other hand, the GO films can be transferred from the air-water interface onto solids by the Langmuir-Blodgett or Langmuir Schaeffer methodologies. Therefore, it is also necessary to study the influence of structure and rheology of different states at the fluid interface on the transfer process and the solid coverage. Just understanding the influence of all these factors on the structure and properties of GO films, it is possible to design films with the necessary properties to stabilize emulsions and foams, or to be transferred to solids as components of biosensors, gas sensors, transparent electrodes and photovoltaic cells.

Declaration of Competing Interest

The authors declare that they have no known competing financial interests or personal relationships that could have appeared to influence the work reported in this paper.

Acknowledgment

The work was founded by European Regional Development Fund, ERDF, Junta de Castilla y León (SA256P18) and MINECO (CTQ2016-78895-R). D.L-D thanks Junta de Castilla y León for financing his postdoc position.

References

[1] Brodie BC. On the atomic weight of graphite. Philos Trans R Soc Lond A 1859;149:249–55.
[2] Geim AK. Graphene: status and prospects. Science 2009;324:1530–4.
[3] Rozada R, Paredes JI, López MJ, Villar-Rodil S, Cabria I, Alonso JA, et al. From graphene oxide to pristine graphene: revealing the inner workings of the full structural restoration. Nanoscale 2015;7:2374–90.
[4] Chua CK, Pumera M. Chemical reduction of graphene oxide: a synthetic chemistry viewpoint. Chem Soc Rev 2014;43:291–312.
[5] Martín-García B, Velázquez MM, Rossella F, Bellani V, Diez E, García Fierro JL, et al. Functionalization of reduced graphite oxide sheets with a Zwitterionic surfactant. ChemPhysChem 2012;13:3682–90.
[6] Claramunt S, Varea A, López-Díaz D, Velázquez MM, Cornet A, Cirera A. The importance of Interbands on the interpretation of the Raman Spectrum of Graphene oxide. J Phys Chem C 2015;119:10123–9.
[7] Eda G, Lin Y-Y, Miller S, Chen C-W, Su W-F, Chhowalla M. Transparent and conducting electrodes for organic electronics from reduced graphene oxide. Appl Phys Lett 2008;92:233305.
[8] Saha SK, Bhaumik S, Maji T, Mandal TK, Pal AJ. Solution-processed reduced graphene oxide in light-emitting diodes and photovoltaic devices with the same pair of active materials. RSC Adv 2014;4:35493–9.
[9] Yin Z, Sun S, Salim T, Wu S, Huang X, He Q, et al. Organic photovoltaic devices using highly flexible reduced Graphene oxide films as transparent electrodes. ACS Nano 2010;4:5263–8.
[10] Alonso-Cristobal P, Vilela P, El-Sagheer A, Lopez-Cabarcos E, Brown T, Muskens OL, et al. Highly sensitive DNA sensor based on Upconversion nanoparticles and Graphene oxide. ACS Appl Mater Interfaces 2015;7:12422–9.
[11] Mendez-Gonzalez D, Calderón OG, Melle S, González-Izquierdo J, Bañares L, López-Díaz D, et al. Contribution of resonance energy transfer to the luminescence quenching of upconversion nanoparticles with graphene oxide. J Colloid Interface Sci 2020;575:119–29.
[12] Fu K, Wang Y, Yan C, Yao Y, Chen Y, Dai J, et al. Graphene oxide-based electrode inks for 3D-printed lithium-ion batteries. Adv Mater 2016;28:2587–94.
[13] Liu J, Cui L, Losic D. Graphene and graphene oxide as new nanocarriers for drug delivery applications. Acta Biomater 2013;9:9243–57.

[14] Yogesh GK, Shuaib EP, Roopmani P, Gumpu MB, Krishnan UM, Sastikumar D. Synthesis, characterization and bioimaging application of laser-ablated graphene-oxide nanoparticles (nGOs). Diamond Relat Mater 2020;104:107733.
[15] Potts JR, Dreyer DR, Bielawski CW, Ruoff RS. Graphene-based polymer nanocomposites. Polymer 2011;52:5–25.
[16] Loh KP, Bao Q, Eda G, Chhowalla M. Graphene oxide as a chemically tunable platform for optical applications. Nat Chem 2010;2:1015–24.
[17] Prezioso S, Perrozzi F, Giancaterini L, Cantalini C, Treossi E, Palermo V, et al. Graphene oxide as a practical solution to high sensitivity gas sensing. J Phys Chem C 2013;117:10683–90.
[18] Kim F, Cote LJ, Huang J. Graphene oxide: surface activity and two-dimensional assembly. Adv Mater 2010;22:1954–8.
[19] Kim J, Cote LJ, Kim F, Yuan W, Shull KR, Huang J. Graphene oxide sheets at interfaces. J Am Chem Soc 2010;132:8180–6.
[20] McCoy TM, Pottage MJ, Tabor RF. Graphene oxide-stabilized oil-in-water emulsions: pH-controlled dispersion and flocculation. J Phys Chem C 2014;118:4529–35.
[21] Jalani G, Jeyachandran D, Bertram Church R, Cerruti M. Graphene oxide-stabilized perfluorocarbon emulsions for controlled oxygen delivery. Nanoscale 2017;9:10161–6.
[22] Yoon KY, An SJ, Chen Y, Lee JH, Bryant SL, Ruoff RS, et al. Graphene oxide nanoplatelet dispersions in concentrated NaCl and stabilization of oil/water emulsions. J Colloid Interface Sci 2013;403:1–6.
[23] Thickett SC, Zetterlund PB. Graphene oxide (GO) nanosheets as oil-in-water emulsion stabilizers: influence of oil phase polarity. J Colloid Interface Sci 2015;442:67–74.
[24] AfzaliTabar M, Alaei M, Bazmi M, Ranjineh Khojasteh R, Koolivand-Salooki M, Motiee F, et al. Facile and economical preparation method of nanoporous graphene/silica nanohybrid and evaluation of its Pickering emulsion properties for chemical enhanced oil recovery (C-EOR). Fuel 2017;206:453–66.
[25] Dao TD, Erdenedelger G, Jeong HM. Water-dispersible graphene designed as a Pickering stabilizer for the suspension polymerization of poly(methyl methacrylate)/graphene core–shell microsphere exhibiting ultra-low percolation threshold of electrical conductivity. Polymer 2014;55:4709–19.
[26] Maithya OM, Li X, Feng X, Sui X, Wang B. Microencapsulated phase change material via Pickering emulsion stabilized by graphene oxide for photothermal conversion. J Mater Sci 2020;55:7731–42.
[27] Zhu J, Wang F, Li D, Zhai J, Liu P, Zhang W, et al. Amine functionalized Graphene oxide stabilized Pickering emulsion for highly efficient Knoevenagel condensation in aqueous medium. Catal Lett 2020;150:1909–22.
[28] Wu H, Yi W, Chen Z, Wang H, Du Q. Janus graphene oxide nanosheets prepared via Pickering emulsion template. Carbon 2015;93:473–83.
[29] He Y, Wu F, Sun X, Li R, Guo Y, Li C, et al. Factors that affect Pickering emulsions stabilized by Graphene oxide. ACS Appl Mater Interfaces 2013;5:4843–55.
[30] McCoy TM, Holt SA, Rozario AM, Bell TDM, Tabor RF. Surfactant-enhanced adsorption of Graphene oxide for improved emulsification of oil in water. Adv Mater Interfaces 2017;4:1700803.
[31] Che Man SH, Ly D, Whittaker MR, Thickett SC, Zetterlund PB. Nano-sized graphene oxide as sole surfactant in miniemulsion polymerization for nanocomposite synthesis: effect of pH and ionic strength. Polymer 2014;55:3490–7.
[32] Barrabino A, Holt T, Lindeberg E. An evaluation of Graphene oxides as possible foam stabilizing agents for CO2 based enhanced oil recovery. Nanomaterials 2018;8:603.
[33] Fang S, Chen T, Chen B, Xiong Y, Zhu Y, Duan M. Graphene oxide at oil-water interfaces: adsorption, assembly & demulsification. Colloids Surf A Physicochem Eng Asp 2016;511:47–54.
[34] Yuan Q, Xue H, Lv J, Wang J, Shi S, Russell TP, et al. Size-dependent interfacial assembly of Graphene oxide at water–oil interfaces. J Phys Chem B 2020;124:4835–42.
[35] Tkacz R, Oldenbourg R, Mehta SB, Miansari M, Verma A, Majumder M. pH dependent isotropic to nematic phase transitions in graphene oxide dispersions reveal droplet liquid crystalline phases. Chem Commun 2014;50:6668–71.
[36] Cote LJ, Kim J, Tung VC, Luo J, Kim F, Huang J. Graphene oxide as surfactant sheets. Pure Appl Chem 2010;83:95.
[37] Kim J, Cote LJ, Huang J. Two dimensional soft material: new faces of Graphene oxide. Acc Chem Res 2012;45:1356–64.
[38] Kim JE, Han TH, Lee SH, Kim JY, Ahn CW, Yun JM, et al. Graphene Oxide Liquid Crystals. Angew Chem Int Ed 2011;50:3043–7.
[39] Narayan R, Kim JE, Kim JY, Lee KE, Kim SO. Graphene oxide liquid crystals: discovery. Evol Appl Adv Mater 2016;28:3045–68.
[40] McCoy TM, Turpin G, Teo BM, Tabor RF. Graphene oxide: a surfactant or particle? Curr Opin Colloid Interface Sci 2019;39:98–109.
[41] Velázquez MM, Ortega F, Monroy F, Rubio RG, Pegiadou S, Pérez L, et al. Langmuir monolayers of the zwitterionic surfactant hexadecyl 1-N-l-tryptophan glycerol ether. J Colloid Interface Sci 2005;283:144–52.
[42] López-Díaz D, García-Mateos I, Velázquez MM. Surface properties of mixed monolayers of sulfobetaines and ionic surfactants. J Colloid Interface Sci 2006;299:858–66.
[43] Valtierrez-Gaytan C, Ismail I, Macosko C, Stottrup BL. Interfacial activity of graphene oxide: anisotropy, loading efficiency and pH-tunability. Colloids Surf A Physicochem Eng Asp 2017;529:434–42.
[44] Shih C-J, Lin S, Sharma R, Strano MS, Blankschtein D. Understanding the pH-dependent behavior of Graphene oxide aqueous solutions: a comparative experimental and molecular dynamics simulation study. Langmuir 2012;28:235–41.
[45] Rong J, Ge M, Fang X, Zhou C. Solution ionic strength engineering as a generic strategy to coat Graphene oxide (GO) on various functional particles and its application in high-performance lithium–Sulfur (Li–S) batteries. Nano Lett 2014;14:473–9.
[46] Staudenmaier L. Verfahren zur Darstellung der Graphitsäure. Berichte der deutschen chemischen Gesellschaft 1898;31:1481–7.
[47] Hofmann U, König E. Untersuchungen über Graphitoxyd. Zeitschrift für anorganische und allgemeine Chemie 1937;234:311–36.
[48] Hummers WS, Offeman RE. Preparation of Graphitic Oxide. J Am Chem Soc 1958;80:1339.
[49] Marcano DC, Kosynkin DV, Berlin JM, Sinitskii A, Sun Z, Slesarev A, et al. Improved synthesis of Graphene oxide. ACS Nano 2010;4:4806–14.
[50] Marcano DC, Kosynkin DV, Berlin JM, Sinitskii A, Sun Z, Slesarev AS, et al. Correction to improved synthesis of graphene oxide. ACS Nano 2018;12:2078.
[51] Chua CK, Sofer Z, Pumera M. Graphite oxides: effects of permanganate and chlorate oxidants on the oxygen composition. Chem A Eur J 2012;18:13453–9.
[52] López-Díaz D, López Holgado M, García-Fierro JL, Velázquez MM. Evolution of the Raman Spectrum with the chemical composition of Graphene oxide. J Phys Chem C 2017;121:20489–97.
[53] Dimiev A, Kosynkin DV, Alemany LB, Chaguine P, Tour JM. Pristine graphite oxide. J Am Chem Soc 2012;134:2815–22.
[54] Dimiev AM, Tour JM. Mechanism of Graphene oxide formation. ACS Nano 2014;8:3060–8.
[55] He H, Riedl T, Lerf A, Klinowski J. Solid-state NMR studies of the structure of graphite oxide. J Phys Chem 1996;100:19954–8.
[56] Lerf A, He H, Riedl T, Forster M, Klinowski J. 13C and 1H MAS NMR studies of graphite oxide and its chemically modified derivatives. Solid State Ion 1997;101–103:857–62.
[57] Lerf A, He H, Forster M, Klinowski J. Structure of graphite oxide revisited‖. J Phys Chem B 1998;102:4477–82.
[58] Gao W, Alemany LB, Ci L, Ajayan PM. New insights into the structure and reduction of graphite oxide. Nat Chem 2009;1:403–8.
[59] Rourke JP, Pandey PA, Moore JJ, Bates M, Kinloch IA, Young RJ, et al. The real Graphene oxide revealed: stripping the oxidative debris from the Graphene-like sheets. Angew Chem Int Ed 2011;50:3173–7.
[60] Su C, Acik M, Takai K, Lu J, Hao S-J, Zheng Y, et al. Probing the catalytic activity of porous graphene oxide and the origin of this behaviour. Nat Commun 2012;3:1298.
[61] Helen R, Thomas SPD, William E, Woodruff Cristina Vallés, Young Robert J, Kinloch Ian A, et al. Deoxygenation of Graphene oxide: reduction or cleaning? Chem Mater 2013;25:3580–8.
[62] Chen X, Chen B. Direct observation, molecular structure, and location of oxidation debris on Graphene oxide Nanosheets. Environ Sci Technol 2016;50:8568–77.
[63] Guo Z, Wang S, Wang G, Niu Z, Yang J, Wu W. Effect of oxidation debris on spectroscopic and macroscopic properties of graphene oxide. Carbon 2014;76:203–11.
[64] Li D, Muller MB, Gilje S, Kaner RB, Wallace GG. Processable aqueous dispersions of graphene nanosheets. Nat Nanotechnol 2008;3:101–5.
[65] Paredes JI, Villar-Rodil S, Martínez-Alonso A, Tascón JMD. Graphene oxide dispersions in organic solvents. Langmuir 2008;24:10560–4.
[66] Thomas HR, Vallés C, Young RJ, Kinloch IA, Wilson NR, Rourke JP. Identifying the fluorescence of graphene oxide. J Mater Chem C 2013;1:338–42.
[67] Bonanni A, Ambrosi A, Chua CK, Pumera M. Oxidation debris in Graphene oxide is responsible for its inherent Electroactivity. ACS Nano 2014;8:4197–204.
[68] Thomas HR, Valles C, Young RJ, Kinloch IA, Wilson NR, Rourke JP. Identifying the fluorescence of graphene oxide. J Mater Chem C 2013;1:338–42.
[69] Tian W, Li W, Yu W, Liu X. A review on lattice defects in graphene: types, generation, effects and regulation. Micromachines (Basel) 2017;8:163.
[70] Huang PY, Ruiz-Vargas CS, van der Zande AM, Whitney WS, Levendorf MP, Kevek JW, et al. Grains and grain boundaries in single-layer graphene atomic patchwork quilts. Nature 2011;469:389–92.
[71] Ferrari AC, Robertson J. Interpretation of Raman spectra of disordered and amorphous carbon. Phys Rev B 2000;61:14095–107.
[72] Ferrari AC, Meyer JC, Scardaci V, Casiraghi C, Lazzeri M, Mauri F, et al. Raman Spectrum of Graphene and Graphene layers. Phys Rev Lett 2006;97:187401.
[73] Casiraghi C, Hartschuh A, Qian H, Piscanec S, Georgi C, Fasoli A, et al. Raman spectroscopy of Graphene edges. Nano Lett 2009;9:1433–41.
[74] Cançado LG, Jorio A, Ferreira EHM, Stavale F, Achete CA, Capaz RB, et al. Quantifying defects in Graphene via Raman spectroscopy at different excitation energies. Nano Lett 2011;11:3190–6.
[75] Saito R, Jorio A, Souza Filho AG, Dresselhaus G, Dresselhaus MS, Pimenta MA. Probing phonon dispersion relations of graphite by double resonance Raman scattering. Phys Rev Lett 2001;88:027401.
[76] Pimenta MA, Dresselhaus G, Dresselhaus MS, Cancado LG, Jorio A, Saito R. Studying disorder in graphite-based systems by Raman spectroscopy. Phys Chem Chem Phys 2007;9:1276–90.
[77] Malard LM, Pimenta MA, Dresselhaus G, Dresselhaus MS. Raman spectroscopy in graphene. Phys Rep 2009;473:51–87.
[78] Ado Jorio RS, Dresselhaus Gene, Dresselhaus Mildred S. Raman spectroscopy in Graphene related systems. Weinheim, Germany: WILEY-VCHVerlag GmbH & Co.; 2011.
[79] Szabó T, Berkesi O, Forgó P, Josepovits K, Sanakis Y, Petridis D, et al. Evolution of surface functional groups in a series of progressively oxidized graphite oxides. Chem Mater 2006;18:2740–9.
[80] Kaniyoor A, Ramaprabhu S. A Raman spectroscopic investigation of graphite oxide derived graphene. AIP Adv 2012;2 032183–13.
[81] Wang L, Zhao J, Sun Y-Y, Zhang SB. Characteristics of Raman spectra for graphene oxide from ab initio simulations. J Chem Phys 2011;135:184503.

[82] Kudin KN, Ozbas B, Schniepp HC, Prud'homme RK, Aksay IA, Car R. Raman spectra of graphite oxide and functionalized Graphene sheets. Nano Lett 2008;8:36–41.
[83] Tuinstra F, Koenig JL. Raman spectrum of graphite. J Chem Phys 1970;53:1126–30.
[84] Vollebregt S, Ishihara R, Tichelaar FD, Hou Y, Beenakker CIM. Influence of the growth temperature on the first and second-order Raman band ratios and widths of carbon nanotubes and fibers. Carbon 2012;50:3542–54.
[85] Sadezky A, Muckenhuber H, Grothe H, Niessner R, Pöschl U. Raman microspectroscopy of soot and related carbonaceous materials: spectral analysis and structural information. Carbon 2005;43:1731–42.
[86] Sze SK, Siddique N, Sloan JJ, Escribano R. Raman spectroscopic characterization of carbonaceous aerosols. Atmos Environ 2001;35:561–8.
[87] Dippel B, Jander H, Heintzenberg J. NIR FT Raman spectroscopic study of flame soot. Phys Chem Chem Phys 1999;1:4707–12.
[88] Venezuela P, Lazzeri M, Mauri F. Theory of double-resonant Raman spectra in graphene: intensity and line shape of defect-induced and two-phonon bands. Phys Rev B 2011;84:035433.
[89] López-Díaz D, Delgado-Notario JA, Clericò V, Diez E, Merchán MD, Velázquez MM. Towards understanding the Raman Spectrum of Graphene oxide: the effect of the chemical composition. Coatings 2020;10:524.
[90] Cote LJ, Kim J, Zhang Z, Sun C, Huang J. Tunable assembly of graphene oxide surfactant sheets: wrinkles, overlaps and impacts on thin film properties. Soft Matter 2010;6:6096–101.
[91] López-Díaz D, Velázquez MM. Blanco de La Torre S, Pérez-Pisonero a, Trujillano R, Fierro JLG, et al. the role of oxidative debris on Graphene oxide films. ChemPhysChem 2013;14:4002–9.
[92] Akbari A, Sheath P, Martin ST, Shinde DB, Shaibani M, Banerjee PC, et al. Large-area graphene-based nanofiltration membranes by shear alignment of discotic nematic liquid crystals of graphene oxide. Nat Commun 2016;7:10891.
[93] Naficy S, Jalili R, Aboutalebi SH, Gorkin Iii RA, Konstantinov K, Innis PC, et al. Graphene oxide dispersions: tuning rheology to enable fabrication. Mater Horizons 2014;1:326–31.
[94] Del Giudice F, Shen AQ. Shear rheology of graphene oxide dispersions. Curr Opin Chem Eng 2017;16:23–30.
[95] Xu Z, Gao C. Aqueous liquid crystals of Graphene oxide. ACS Nano 2011;5:2908–15.
[96] Aboutalebi SH, Gudarzi MM, Zheng QB, Kim J-K. Spontaneous formation of liquid crystals in Ultralarge Graphene oxide dispersions. Adv Funct Mater 2011;21:2978–88.
[97] Hogan BT, Kovalska E, Craciun MF, Baldycheva A. 2D material liquid crystals for optoelectronics and photonics. J Mater Chem C 2017;5:11185–95.
[98] Dan B, Behabtu N, Martinez A, Evans JS, Kosynkin DV, Tour JM, et al. Liquid crystals of aqueous, giant graphene oxide flakes. Soft Matter 2011;7:11154–9.
[99] Koltonow AR, Luo C, Luo J, Huang J. Graphene oxide sheets in solvents: to crumple or not to crumple? ACS Omega 2017;2:8005–9.
[100] McCoy TM, de Campo L, Sokolova AV, Grillo I, Izgorodina EI, Tabor RF. Bulk properties of aqueous graphene oxide and reduced graphene oxide with surfactants and polymers: adsorption and stability. Phys Chem Chem Phys 2018;20:16801–16.
[101] Imperiali L, Liao K-H, Clasen C, Fransaer J, Macosko CW, Vermant J. Interfacial rheology and structure of tiled Graphene oxide sheets. Langmuir 2012;28:7990–8000.
[102] Roberts GG. Langmuir-Blodgett Films. Oxford U.K: Springer Science; 1990.
[103] Petty MC. Langmuir—Blodgett films: An introduction. Cambridge University Press; 1996.
[104] Cote LJ, Kim F, Huang J. Langmuir—Blodgett assembly of graphite oxide single layers. J Am Chem Soc 2009;131:1043–9.
[105] Hidalgo RS, López-Díaz D, Velázquez MM. Graphene oxide thin films: influence of chemical structure and deposition methodology. Langmuir 2015;31:2697–705.
[106] López-Díaz D, Merchán MD, Velázquez MM, Maestro A. Understanding the role of oxidative debris on the structure of Graphene oxide films at the air-water Interface: a neutron reflectivity study. ACS Appl Mater Interfaces 2020;12:25453–63.
[107] Fainerman VB, Kovalchuk VI, Lucassen-Reynders EH, Grigoriev DO, Ferri JK, Leser ME, et al. Surface-pressure isotherms of monolayers formed by microsize and Nanosize particles. Langmuir 2006;22:1701–5.
[108] Fainerman VB, Lucassen-Reynders EH, Miller R. Description of the adsorption behaviour of proteins at water/fluid interfaces in the framework of a two-dimensional solution model. Adv Colloid Interface Sci 2003;106:237–59.
[109] Lackinger M, Heckl WM. Carboxylic acids: versatile building blocks and mediators for two-dimensional Supramolecular self-assembly. Langmuir 2009;25:11307–21.
[110] Braun L, Uhlig M, von Klitzing R, Campbell RA. Polymers and surfactants at fluid interfaces studied with specular neutron reflectometry. Adv Colloid Interface Sci 2017;247:130–48.
[111] Campbell RA. Recent advances in resolving kinetic and dynamic processes at the air/water interface using specular neutron reflectometry. Curr Opin Colloid Interface Sci 2018;37:49–60.
[112] Vorobiev A, Dennison A, Chernyshov D, Skrypnychuk V, Barbero D, Talyzin AV. Graphene oxide hydration and solvation: an in situ neutron reflectivity study. Nanoscale 2014;6:12151–6.
[113] Klechikov A, Sun J, Vorobiev A, Talyzin AV. Swelling of thin Graphene oxide films studied by in situ neutron reflectivity. J Phys Chem C 2018;122:13106–16.
[114] Bonatout N, Muller F, Fontaine P, Gascon I, Konovalov O, Goldmann M. How exfoliated graphene oxide nanosheets organize at the water interface: evidence for a spontaneous bilayer self-assembly. Nanoscale 2017;9:12543–8.
[115] Razavi S, Cao KD, Lin B, Lee KYC, Tu RS, Kretzschmar I. Collapse of particle-laden interfaces under compression: buckling vs particle expulsion. Langmuir 2015;31:7764–75.